





The Photo-Oxidation of CO from Ambient Air Using Catalytic Asphaltic Pavement

Seba S. Mohammed^a , Zainab Y. Shnian^b, Mohammad F. Abid^c, Asawer Alwasiti^{*a} ,
Kadhim Noori Abed^c, Mohammed I. Mohammed^d, Zainab Hameed^c, Sajda S. Faris^e, Peter
Philib^f

^a Institute of Northern Technical University, Department of Chemical and Oil Industries, Mosul, Iraq.

^b Chemical Engineering Dept., University of Technology-Iraq, Alsina'a street, 10066 Baghdad, Iraq.

^c Al-Turath University College, Department of Oil & Gas Refining Engineering, Baghdad, Iraq; .

^d Al-Hikma University College, Department of Medical Instrumentation Techniques Engineering, Baghdad.

^e Mechanical Engineering Dept., University of Technology-Iraq, Alsina'a street, 10066 Baghdad, Iraq.

^f Mechanical Engineering and Energy Processes, Southern Illinois University, USA.

*Corresponding author Email: asawer.a.alwasiti@uotechnology.edu.iq

HIGHLIGHTS

- The effectiveness of the oxidation of carbon dioxide gas emitted by an internal combustion engine was studied.
- The CO conversion positively depends on Cu loading, light intensity, and relative humidity.
- The best photo-oxidation efficiency of 56.4% was achieved after three hours of operation.

ARTICLE INFO

Handling editor: Qusay F. Alsahy

Keywords:

Carbon monoxide; Air quality; Copper doped Titanium oxide; asphaltic pavement; photooxidation.

ABSTRACT

Road transportation in urban areas may be considered a major source of environmental pollution. The purpose of this study is to determine the effectiveness of the oxidation of carbon dioxide gas emitted by an internal combustion engine. This is achieved using an asphaltic pavement coated with Cu/TiO₂ nanoparticles by spraying and irradiating with white light under ambient conditions to reduce the air pollution problem (carbon monoxide) caused by vehicles. Using electron microscopy, energy dispersive spectroscopy, and Fourier transform infrared spectroscopy, we determined the physicochemical and morphological characteristics of the photocatalyst. Following the characterization study, the photo-catalytic activity of the asphalt materials was determined. Experimental results showed that CO conversion positively depends on different conditions, including Cu loading, light intensity, and relative humidity. However, the gas flow rate showed a different trend. The optimal operating parameters were determined as follows: Cu loading (3.6% by weight), a flow rate of gas (1 L/min), relative humidity (30%), and light intensity (35 W/m²) to ensure the best photo-oxidation efficiency of 56.4% after three hours of operation. A mathematical correlation related to CO₂ removal as a function of different operating conditions was found with a correlation factor of 0.975 and a variance equal to 0.964. Moreover, a kinetic pathway for photo-oxidation of CO at various oxygen concentrations was presented.

1. Introduction

Today, the emission of carbon monoxide discharged into the atmosphere due to fuel combustion is one of the most significant emissions concerns in the world. In general, the transport sector has a negative effect on air quality. It can considerably raise the risk of respiratory illness [1]. Consequently, it is advisable to keep these contaminants to a minimum. The advanced oxidation process of carbon monoxide by photoreaction, which depends on semiconductor materials, can be another method of removing carbon monoxide. The advantage of this technique is that it can be successful in ambient conditions and can be simultaneously used for different gaseous pollutants such as volatile organic compounds, which is very convenient at the same time [2]. The share of energy-consuming sectors in pollutant emissions in 2009 is listed in Table 1 [3].

Table 1: Sharing of energy-consuming activities in pollutant emissions in 2009 [3]

Portion gas	N ₂ O	CH ₄	CO ₂	SPM	CO	SO ₃	SO ₂	NO _x
Homes tic, Commercial, and public	4.5	8	25.7	2.9	0.6	7.8	6.5	6.7
Industry	2.7	4.2	15.8	4.6	0.4	30.2	20.5	9.0
Transportation	48.0	87.7	24.9	78.1	96.9	38.9	32.4	49.6
Agro commercial	40.2	1.6	2.5	8.0	0.3	2.6	4.4	39
Refinery	0.4	0.7	3.2	-----	-----	-----	-----	-----
Powerhouse	4.2	6.6	27.9	6.3	1.8	20.4	36.3	30.7
Total	100	100	100	100	100	100	100	100

Table 1 shows that traffic shares a higher portion of the air pollution due to gaseous CO. TiO₂ is a semiconductor that is often studied in photo-catalytic techniques [4, 5] because it has excellent properties like a strong ability to oxidize, a low price, and is non-toxic and chemically inert. The photocatalysis techniques use TiO₂ and the UV spectrum. The band energies of TiO₂ are close to 3.21 eV. Pure TiO₂ absorbs the UV spectrum and initiates photo-degradation. Hence, the delphinium band energy of 3.2 eV must be overcome. For example, a lot of work has been done to move TiO₂ catalysis into the visible region by lowering the band energy level. This allows solar light to be used for photolysis. Because of this, one of the most interesting things to study is how to change materials to change the band-gap. Most of the time, the photocatalytic properties of TiO₂ are changed by coating it with metal oxide and depositing it on the surface. This is done to make use of the visible light wavelength [7]. Called "defect engineering," the modification process can create a range of modifications in TiO₂ particles, thus imparting new properties such as a reduced band gap and visible-light-induced photo-catalytic activities. In the present work, this technique was used by depositing CuO with a narrow band energy level (1.4–2.3 eV) on the surface of TiO₂, which has a band-gap energy of 3.21 eV for wavelengths of 386 nm, to obtain Cu-doped TiO₂, which has a band-gap energy of 2.27 eV for wavelengths of 546 nm. This decrease in band-gap energy shifts wavelengths from the ultraviolet to the visible region. Cu loading increases with the changes in band-gap energy and wavelength and TiO₂-conjugated Cu shows more stability with higher photo-catalytic activity in visible light ($\lambda > 400$ nm) [8]. This process involves no expense as it occurs at room temperature under atmospheric pressure. It is relatively green compared to other methodologies, which makes this modification method highly efficient, practical, and economical [5].

The enhancement in photocatalytic performance is derived from the increase in specific surface area, providing more reaction sites and increasing the conversion between Cu²⁺ and Cu⁺, increasing the separation rate of photogenerated pairs with the lowest recombination rate [9, 10]. So, TiO₂ with a metal framework is vital and active in various photoreactions [11].

There are some studies on the photocatalytic activity of CO oxidation in the literature [12]. Li et al. [13] studied the oxidation of CO on Pt/TiO₂ irradiated by UV light. Selishchev et al. [14] studied the effects of Pd/TiO₂ catalysts that completely oxidized CO to CO₂ at room temperature with UV-LED irradiation. Tosun et al. determined the effectiveness of photo-catalytic asphalt material, enhanced by solar rays, by applying nano-sized titanium dioxide (TiO₂) under suitable heat treatment to reduce CO-carbon monoxide with a removal efficiency of 69.02% [15]. Under UV light, Kolobov and coworkers found that Pd/TiO₂ presented a 3-fold CO oxidation rate under UV light compared with darkness (10 ppm/min) [16]. Various published data on experimental CO conversion by photocatalysis using doped semiconductors can be summarised in Table 2. The utilization of simulated solar light for the photo-catalytic oxidation of organic pollutants onto Cu/TiO₂ is explained in a few works of literature [9, 17].

Table 2: Photocatalysis Researches on CO oxidation

Catalyst	Irradiation	Temp.(°C)	%CO Conversion	Ref.
Pd/ TiO ₂	UV	25	100 (0.33 h)20	[14]
Pt/ TiO ₂	UV	20	100 (0.5 h)	[18]
Au/ TiO ₂	Visible	20-21	38.5	[19]
RuO ₂ / TiO ₂ /Pt	UV	20	100 (1 hr)	[20]
ZIF-8/Au/ TiO ₂	Solar(visible)	20	42.5	[21]
Au/ TiO ₂ @CuO	Solar(visible)	20	70	[22]
Au/Al ₂ O ₃	Solar(visible)	20	25.1	[23]
TiO ₂ -supported Pt/Co-B	(UV) +thermal	50-100	90-100	[24]
Au/ TiO ₂	Solar(visible) +thermal	50	100	[25]
Pd/N- TiO ₂	Solar(visible) +thermal	20- 100	100	[26]
Pt/CeO ₂ - TiO ₂	(UV)+thermal	60- 200	90	[27]
Zn doped OMS-2	Solar(visible) +thermal	50- 230	87.5	[28]
Fe ₃ Si/Co ₃ O ₄	Solar(visible) +thermal	160	> 95 %	[29]

The goal of this work was to see if CO from an internal combustion engine could be oxidized by spreading Cu-doped TiO₂ nanoparticles on asphalt pavement and exposing them to simulated solar light. Different parameters such as Cu loading, gas flow rate, light intensity, and relative humidity were investigated for their effect on the process efficiency. Moreover, the probable kinetic pathway of photooxidation of CO was introduced.

2. Materials and Methods

2.1 Materials

The Civil Engineering Department at the University of Technology provided the Marshall Specimens (MS), which were 100 mm in diameter and 55mm in height. The nano-TiO₂ (anatase phase; purity 98.0% min; average particle size of 25nm) was provided by Hongwa International Group Ltd., China. from BDH-Analar, copper sulphate (CuSO₄) was purchased in England. Thomas Bake India supplied an ammonium hydroxide solution (25 wt%). Ethanol (reagent grade) was purchased from Sigma Aldrich, India, and distilled water from Al-Mansour Company, Iraq.

2.2 Methods

2.2.1 Synthesising Cu-doped TiO₂

By making several weight percentages of Cu-doped TiO₂ (1, 3.5, and 5 wt% Cu), the effect of Cu on photocatalyst activity was examined. To create 0.55 M of CuSO₄ solution, 65 g of CuSO₄ and 3.5 wt% Cu-doped TiO₂ were dissolved in an aqueous (NH₄OH) solution (10 wt%). Three hours were spent stirring the prepared mixture at 500 rpm. Five grams of nano-TiO₂ were added during mixing. Then, for 30 minutes, with a 3-minute break in between every 5 minutes of the ultrasonication process, the mixture was subjected to an ultrasound generator (Model WUC-D06H, Ultrasonic Cleaner Set). The mixture was then filtered using two 5-micron filters. To remove the organic components, the residue is first rinsed three times with distilled water and then twice with alcohol. The sediment was dried for two hours at 110°C. After being characterized by SEM and EDX, the dried powder was kept in a sealed container and used in the experimental course.

2.2.2 Coating Method

A certain quantity of TiO₂ in the water was put in a can and sonicated for 5 minutes. As seen in Figure 1, the solution was sprayed on the surface of the Marshall Specimen (MS).



Figure 1: Marshal Specimen (MS) coating

2.2.3 Analysis techniques

Surface features were characterized with an INSPECT S50 (SEM) at an accelerating voltage of 350 V–40 kV; probe current: up to 4 μA, constantly alterable; enlargement: 20 to 106 x. Moreover, the (EDS) INSPECT S50/FEI model was utilized.

2.2.4 Experimental setup

Figure 2 illustrates a drawing of the experimental components, while Figure 3.a shows an image of the experimental setup, including a reactor (No. 7). The reactor is composed of a transparent Plexiglas chamber with dimensions of 0.4 m x 0.4 m x 0.4 m, as shown in the drawing. There is a xenon bulb (No. 10) (HID lamp, input power of 35 watts, and outlet flux of 4000 lumens) inside the reaction chamber. A flow meter (No. 4) (Cologno Monzese, type Cilea 36, flow rate up to 3 L/min). The relative humidity was changed using a humidifier (No. 6) and measured by a humidity meter, model YEM-20L, from Shenzhen Yowexa Sensor System, Ltd. An internal combustion engine (No. 1) was used to produce combustion gases loaded into the reaction chamber. A combustion gas analyzer (No. 8) (Model HFP-0401(BX) from Xi'an Huafan Instrument Co., Ltd.) was used to analyze both the gas exiting from the combustion engine outlet and the reaction chamber outlet. The xenon lamp irradiated the asphalt specimens. CO degradation tests were conducted to evaluate the photocatalytic activity. The gases go along the chamber, where the sprayed MSs by the semiconductor emulsion (Cu-doped TiO₂) reside and are irradiated by the xenon lamp Figure 3.b The gas composition is detected at the system's exit, and the photocatalytic efficacy can be calculated. The physical parameters such as humidity, temperature, light irradiation (wavelength and power), gas flow rate, and gas concentration can be controlled.

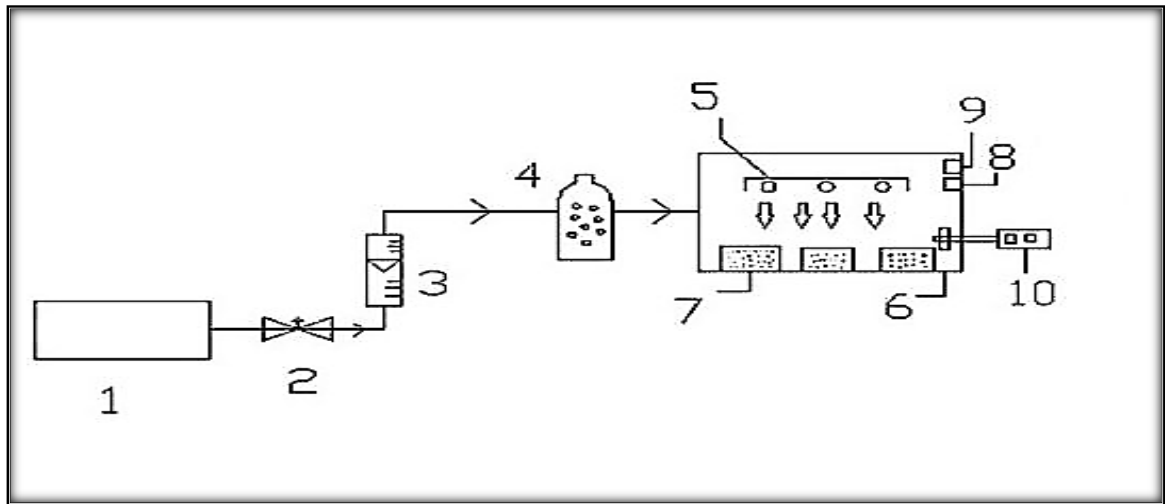


Figure 2: The setup for the experiment. 1- Internal combustion engine 2- Valve. 3- Flow meter. 4- Humidifier. 5- Xenon lamp. 6- Reaction chamber. 7- Marshall Specimens. 8- Temperature sensor. 9- Relative humidity sensor. 10- Gas analyzer



Figure 3: (a) Images of the experimental setup, (b) photocatalytic reactor

3. Results and Discussion

3.1 Catalyst Identification

3.1.1 EDS analysis

EDS can be utilized to determine the elements in a sample [30–31]. The Cu-doped TiO_2 catalysts were distinguished by their surface morphology Figure 4. The x-axis of the EDS image displays the ionization energy, and the y-axis displays the count. The more the count increases, the more this element exists in this area of observance. The existence of Cu metal over TiO_2 is emphasized by comparing TiO_2 that is uncoated (Figure 5a) with TiO_2 coated with 3.6 wt% Cu (Figure 5b). Figure (4a) displays a percentage of TiO_2 and O_2 of 62.5 and 37.5 weight percent, respectively, while Figure (4b) displays a percentage of TiO_2 , O_2 , and Cu of 47.5, 49, and 3.6 weight percent, respectively.

3.1.2 SEM analysis

Scanning electron microscopy (SEM) is widely used in science to characterize the surface roughness of materials [30]. The precise particle size will be quickly determined via SEM track. SEM photographs of 3.5% wt. Cu-doped TiO_2 are shown in Figure 5 a (SEM Mag. 0.6 kx), and SEM photographs of Cu-free TiO_2 are shown in Figure 5 b (SEM Mag. 0.6 kx). On the TiO_2 board, the Cu powder was practically evenly distributed.

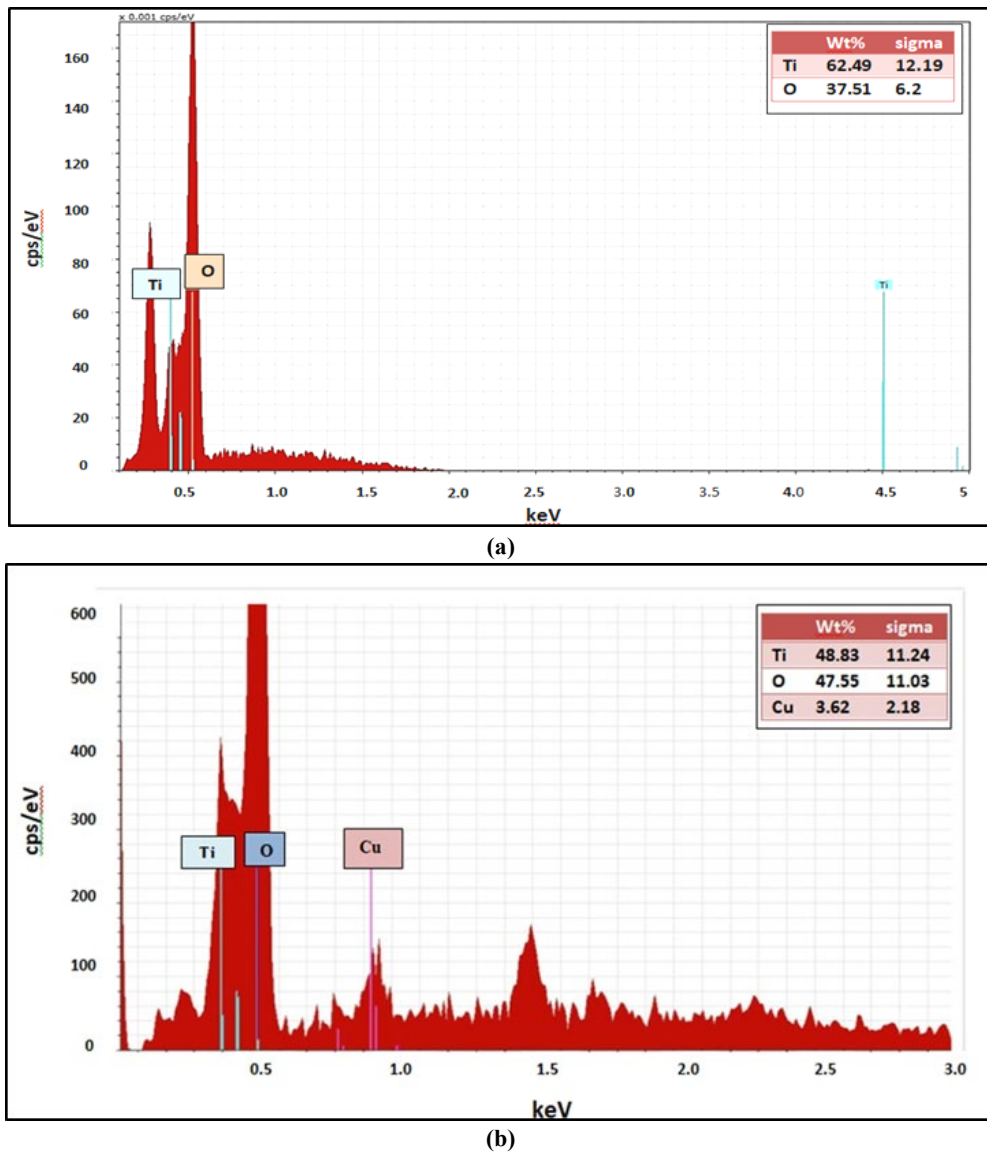


Figure 4: EDS snapshots of (a) Cu-free TiO₂ and (b) 3.6wt% Cu-doped TiO₂

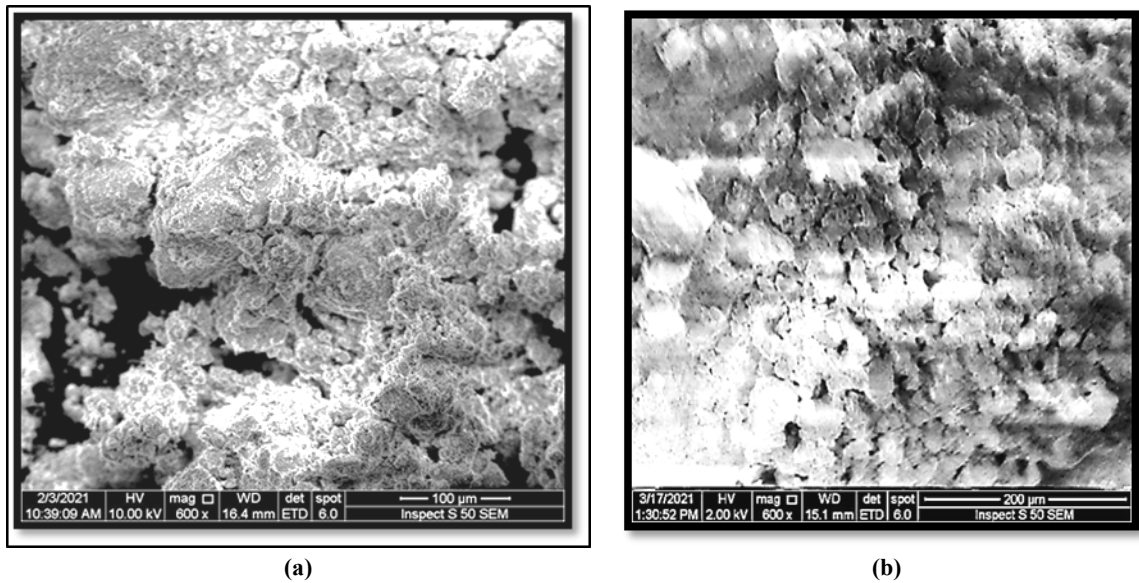


Figure 5: SEM snapshots of (a) Cu-free TiO₂ and (b) 3.6wt% Cu-doped TiO₂

3.1.3 The FTIR Analysis

The FTIR spectrum comparison of pure TiO_2 (Figure 6a) and Cu-TiO_2 (Figure 6b) nanoparticles is shown in Figure 6. As can be seen, the peaks in the pure TiO_2 sample at 3430 cm^{-1} and 1822 cm^{-1} are caused by the stretching and bending vibrations of the OH group caused by water molecules. At 3450 cm^{-1} and 1730 cm^{-1} , the Cu-TiO_2 sample exhibits the same broad bands. For the Cu-TiO_2 sample, the absorption band of this peak occurred around 680 cm^{-1} , confirming the presence of stretching vibrations of the Ti-O bond in the pure TiO_2 sample's peak around 760 cm^{-1} [32]. Moreover, the broad absorption band in the range of $1100\text{--}1400\text{ cm}^{-1}$ for the Cu-TiO_2 sample is connected to the Cu-O vibrations. These findings demonstrated the emergence of Cu-TiO_2 . Also, the pure TiO_2 sample has a greater band number for the OH group than the Cu-TiO_2 sample does, according to the FTIR plot.

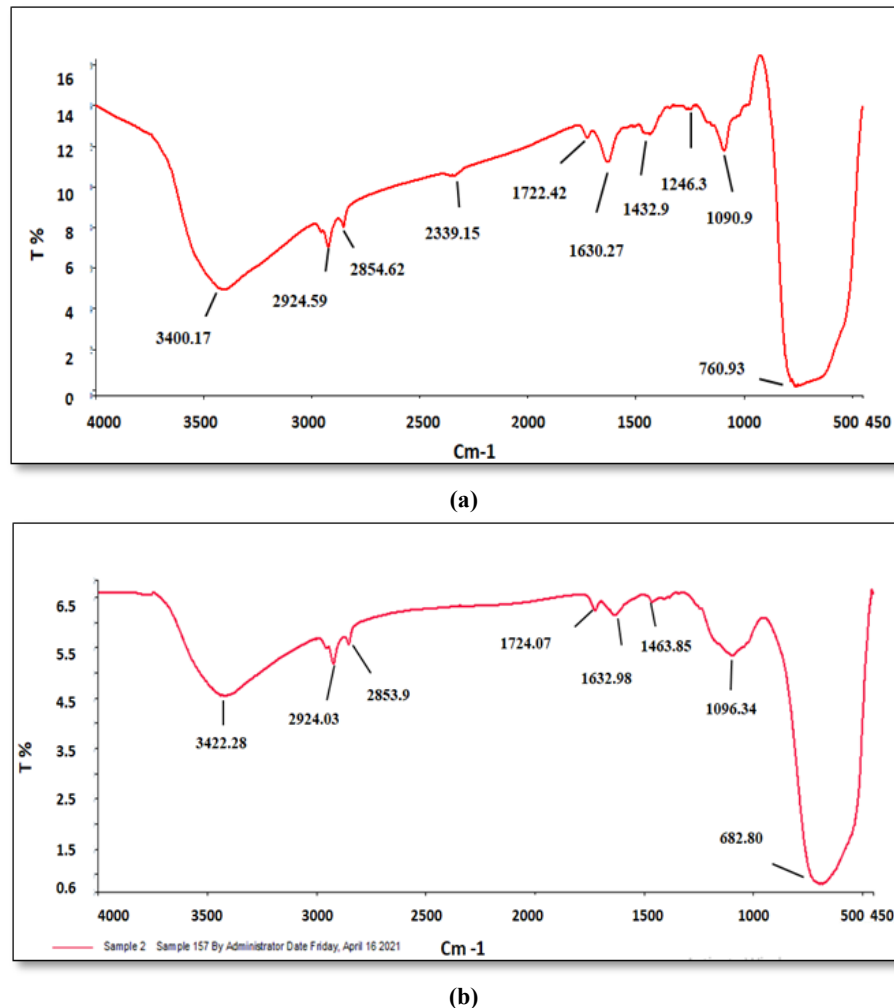


Figure 6: The FTIR spectrum of (a) pure TiO_2 and (b) 3.6wt% Cu-doped TiO_2

3.2 The Effect of Operating Parameters on CO Oxidation

3.2.1 The effect of Cu loading on TiO_2 contact angle

It is well-known that the degree of wettability of TiO_2 nanoparticles enhances the surface photocatalytic activity [33]. In the present work, the effect of Cu loading on the hydrophilicity of TiO_2 nanoparticles was studied. The contact angle meter model (CAM 110-Taiwan) was utilized to measure the water contact angle (WCA); a $5\ \mu\text{L}$ DI water drop was dripped on the catalyst particle. Figure 7 (a, b, c, and d) represents the computer images of contact angles obtained for water sprayed on various copper-loaded specimens. Generally, the literature indicates that if the water contact angle is smaller than 90° , the solid surface is considered hydrophilic. If the water contact angle is greater than 90° , the solid surface is hydrophobic [34]. Table 3 revealed that catalysts of different Cu loadings (0, 1, 3.6, and 5 wt.%) have contact angles of 14.00, 24.02, 49.05, and 58.24 degrees, respectively, indicating that the Cu loading over the specimen surface does not affect the hydrophilicity that helps remove solid pollutants that adhere to surfaces by washing.

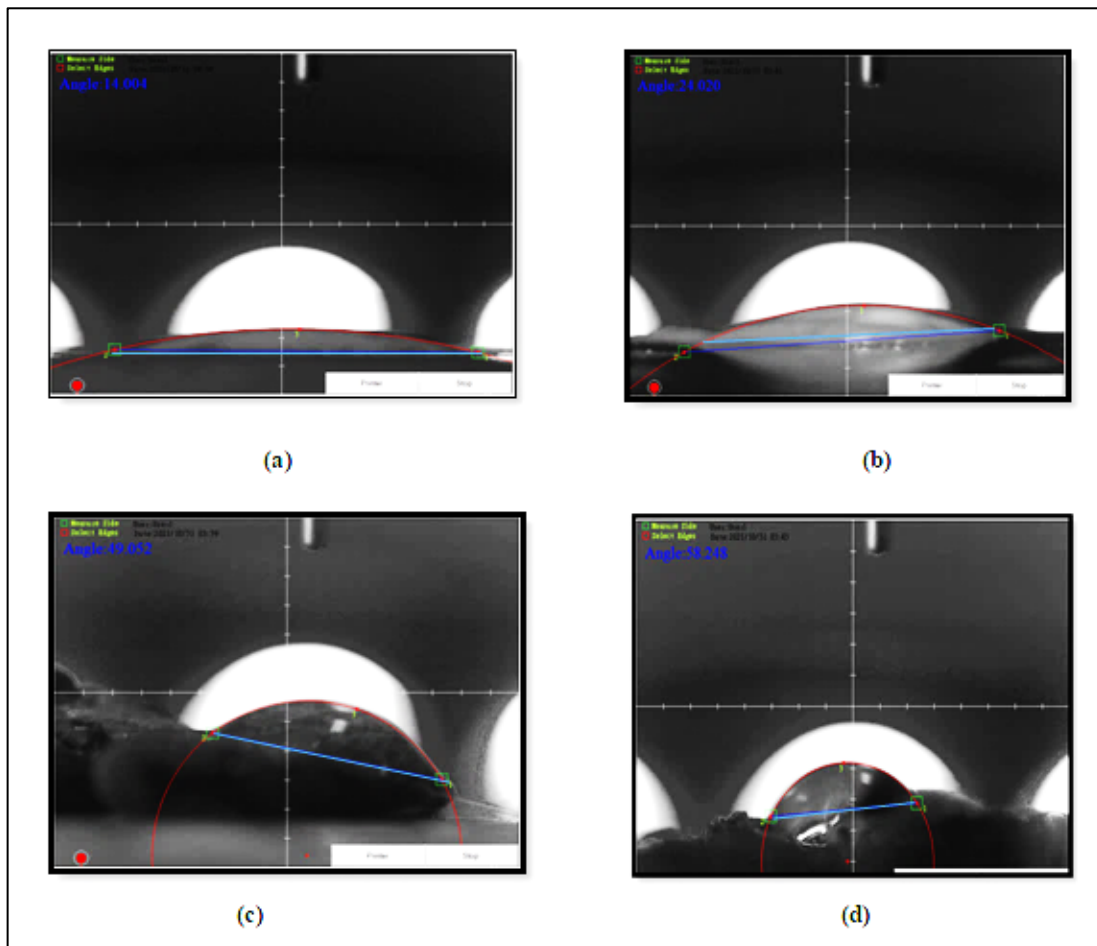


Figure 7: Images of contact angles for (a) Cu-free TiO₂; (b) 1wt% Cu-TiO₂; (c) 3.6 wt. % Cu-TiO₂; (d) 5 wt. % Cu-TiO₂

Table 3: Effect of Cu loading on catalyst's contact angle

Item	wt. % Cu loading	Water contact angle (degree)
1	0	14.00
2	1	24.02
3	3.6	49.05
4	5	58.24

3.2.2 Effect of operating time

Figure 8 plots the variation of CO concentrations versus the operational time at $Q_G = 1$ L/min, $h\nu = 35$ W/m², and relative humidity = 30% both in the presence and absence of the photocatalyst (i.e., 3.6 wt. % Cu-doped TiO₂). Notably, the Japanese standard [35] states that each Marshall sample must be inspected under UV light for a total of 5 hours, including roughly 30 minutes, to guarantee equilibrium concentrations. In the present work, the equilibrium condition is attained after the internal combustion engine has been running for roughly 1.1 hours and before the xenon lamp in the reaction chamber is turned on. Moreover, after three hours of operation, the system established a steady state in the presence or absence of the photocatalyst. Within three hours of illumination in the presence of the photocatalyst, the CO concentration begins to decrease from 700 to 300 ppm. The system effectiveness was calculated by measuring the concentrations of CO after 3 hours and at equilibrium when the light was just switched on, according to Equation 1 [36].

$$\text{CO reduction efficiency} = \frac{\text{CO reduction in concentration after 3 h}}{\text{CO concentration at equilibrium}} \times 100\% \quad (1)$$

In the plot, the carbon monoxide oxidation efficacy of the present work was 56.4% and 24.30% in the presence and absence of the photocatalyst, respectively. This reasonable efficiency affirms the practicality of the operating setup at ambient conditions for CO oxidation.

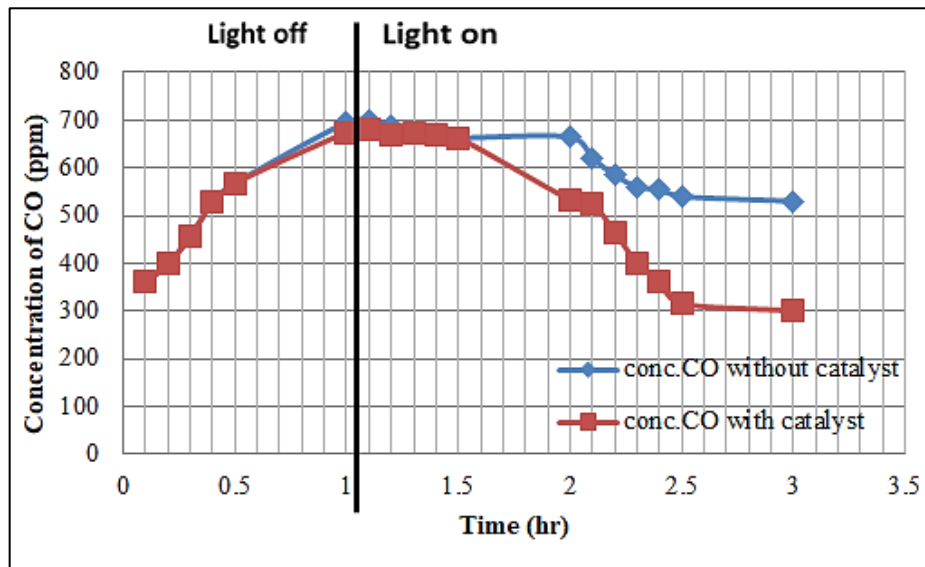


Figure 8: Variation of CO concentrations versus the operational time at $Q_G = 1$ L/min, $h\nu = 35$ (W/m²), relative humidity = 30%, and Cu loading = 3.6wt. %

3.2.3 The effect of gas flow rate

Figure 9 depicts the effect of gas flow rate on CO degradation at time = 3 h, weight percent Cu = 3.6%, and $h\nu = 35$ W/m². The figure shows an inverse link between CO degradation and gas flow rate. The removal of CO decreased from 56.4 to 38.8% when the gas flow rate increased from 1 to 3 L/min. This pattern can be explained by the fact that the reaction rate depends on how long the pollutant has been present in the solar reactor [37]. The CO removal within a specific volume of test gas increases proportionally to its residence time over a photocatalytic surface. The more time that is afforded for pollutants to be absorbed, the more oxidation occurs at the active sites of TiO₂. Our results are in line with the body of published research, which demonstrates a distinct inverse relationship between gaseous pollution removal and gas flow rate [38–39]. However, on-field CO removal can vary greatly depending on the wind speed and direction, which change over time. This implies that the outcomes of the current lab study should be implemented on-site.

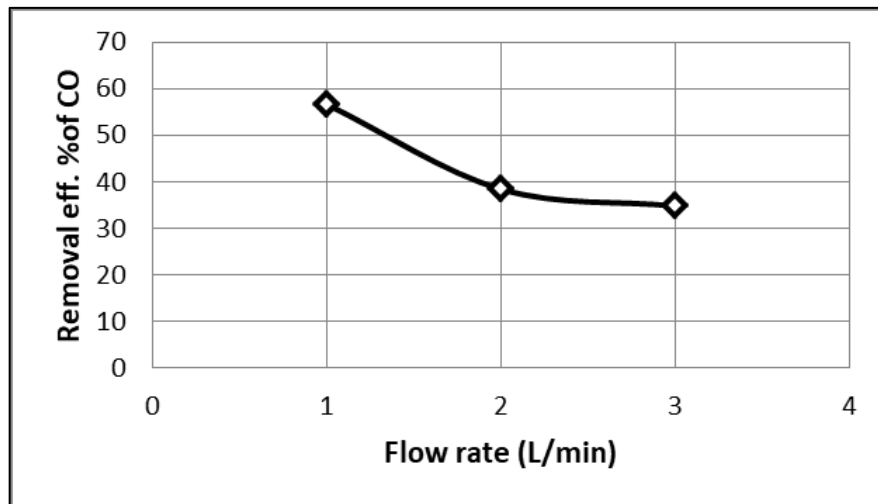


Figure 9: Variation of CO removal percentage against gas flow rate

3.2.4 Effect of air humidity

The influence of relative humidity (%RH) on the removal efficiency (%R) of CO is shown in Figure 10. CO breaks down more quickly when the relative humidity goes from 0 to 30%. However, raising the %RH above 30% has an inverse influence on the %R of CO. As the %RH changed from 0, 10, 30, 50, and 80%, the %R of CO was 6.8, 35, 56.4, 41, and 32.4%. This trend can be elucidated by the effect of concrete pavement, including TiO₂, on the %R of CO occurring when OH radicals oxidize CO. These OH radicals are formed when an (e- and h+) pair oxidizes a hydroxyl ion (OH-) in an H₂O molecule on the TiO₂ surface [33]. This would imply that when the TiO₂ surface is not moistened, the CO rate is nearly negligible (7%). On the other hand, as %RH has increased, approaching (RH = 10%) in the photoreactor, the %R of CO has increased to 35% because more *OH radicals are generated. As more water vapor was introduced, the formation rate increased until a maximum removal of CO (56.4%) was reached with RH = 30%. An opposite behavior of CO removal was noticed after %RH started to rise more.

This indicates that increasing %RH over the optimum rate would cause water molecules to gradually aggregate on the TiO₂ surface, increasing the mass transfer resistance of CO to the TiO₂ active sites on the surface. [40] It is proposed that water molecules on the TiO₂ block photocatalyst active sites.

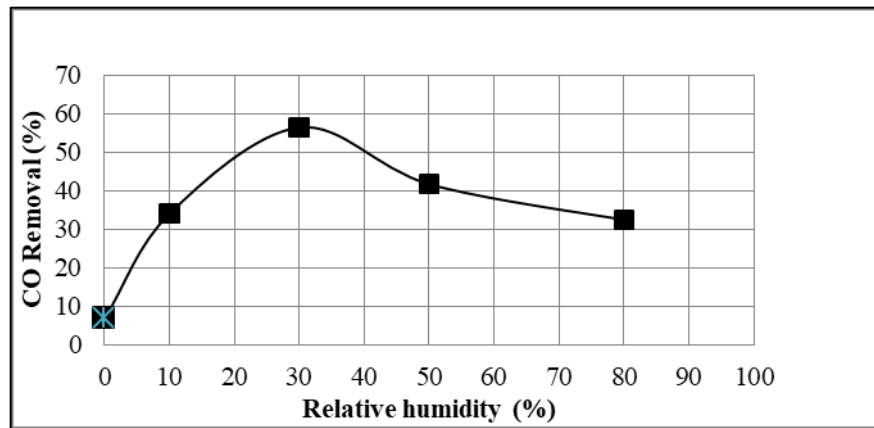


Figure 10: Effect of relative humidity on CO degradation for TiO₂-CU

3.2.5 Effect of light intensity

Figure 11 plots the influence of lamp flux on the %R of CO. Figure shows that increasing the lamp intensity from 35, 50, and 70 W/m² increased the %R of CO by 56.4, 58.5, and 59.5%, respectively. This trend emerges due to the effect of lamp flux on the generation of (e⁻ - h⁺) pairs on the surface of TiO₂. As more (e⁻ - h⁺) pairs were formed, a corresponding number of (*OH) radicals for CO oxidation were also formed. This behavior was reported by [38]. In addition, a linear correlation between light fluxes and the %R of CO was demonstrated below the partition point (i.e., 50 W/m², 58.5%).

In contrast, a non-linear correlation is above this point [41–42]. This is because, in the linear correlation, (e⁻ - h⁺) pairs are filled by reactions with species on the TiO₂ surface (e.g., OH⁻) faster than by rejoining with excited electrons; on the other hand, in the non-linear correlation, holes are filled by recombination at a faster rate than by reactions with other species. This behavior was also found by Jacoby et al. [41]. However, in Figure 12, increasing lamp flux from 35 to 50 W/m² results in a percentage CO degradation of 3.5%, whereas a 1.6% increase in CO degradation is obtained when lamp flux increases from 50 to 70 W/m². This behavior was also revealed by [43], who reported a noticeable enhancement in CO oxidation rate with lamp flux from 10 to 25 W/m². When the lamp flux was increased from 25 to 40 W/m², CO oxidation was not as significant as in the first case.

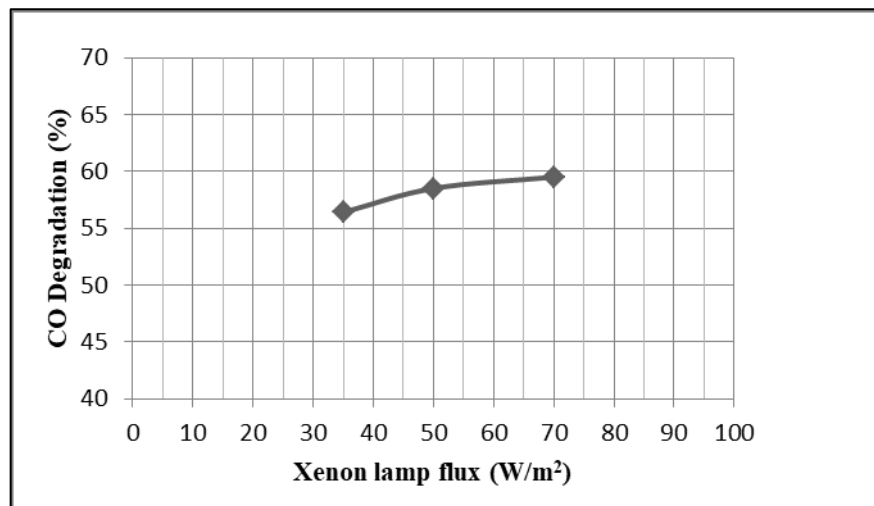


Figure 11: Variation of % CO degradation against Xenon lamp flux for TiO₂-CU

3.2.6 Effect of Cu-doping

The influence of Cu loading on the %R of CO is plotted in Figure 12. It is seen in the figure that as wt. % Cu is raised from 0, 1, 3.5, and 5 wt. %, the % R of CO is boosted from 10, 25, 56.4, and 56.6%, correspondingly. This trend may be due to the impact of wt. % Cu on the bandgap energy of TiO₂, which is reduced as the wt. % Cu is boosted [44]. Shnian et al. [9] found experimentally that the light energy required to generate (e⁻ - h⁺) pairs on TiO₂ is proportional to its bandgap energy. As mentioned earlier, CuO shows a low bandgap (i.e., 1.4 eV). Thus, when CuO is joined with TiO₂, the system shows boosted activity and increased (*OH) radical formation. This explains the enhancement of the Cu-doped TiO₂ activity for boosting the removal of CO. Furthermore, it was observed that boosting Cu from 3.5 to 5% results in no noticeable impact on the %R of

CO. It may be deduced that an optimum ratio of Cu/TiO₂ is required to offer the best photocatalytic activity. The present results agree well with the published data of [45], who prepared Pt/TiO₂ for the oxidation of CO irradiated by a UV lamp.

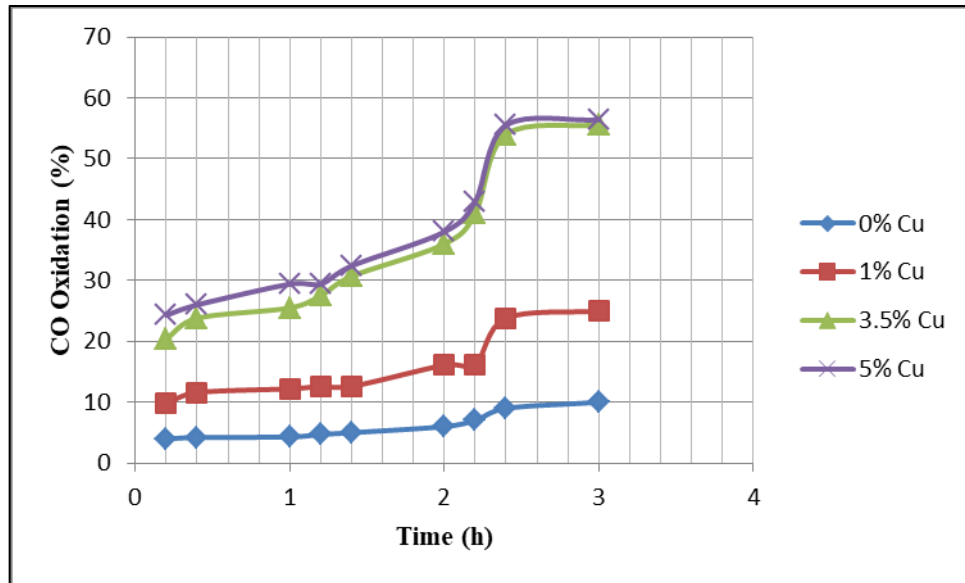
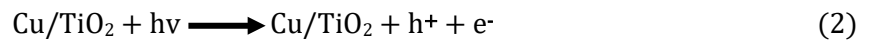


Figure 12: Effect of Cu loading (wt. %) on CO removal

3.3 Kinetic Pathway

For the Cu/TiO₂ catalyst, light irradiation has a high impact linked with the generation of hole-electron (h⁺-e⁻) pairs.

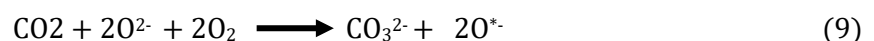


This reaction depicts the photocatalysis operation stimulated by light flux. The e⁻ and h⁺ pairs can oxidize the substrate molecules over the Cu/TiO₂ surface. At low oxygen concentrations, the CO oxidation with humidity, the h⁺ holes can react with H₂O molecules to generate hydroxyl radicals (*OH), which offer high oxidation power and react with CO-producing carboxyl groups. Their degradation generates CO₂ and H₂.



From (Equation 4), it is worth noting that high numbers of *OH radicals result in higher CO oxidation. Another example is the (e⁻ - h⁺) pair generation mechanism over Cu/TiO₂. The bandgap of TiO₂ is 3.2 eV, permitting the electron to be conveyed from the valence energy level to the conduction energy level under UV radiation. The UV spectrum participates in about 5% of the total light spectrum [46]. This implies that the reaction rate (Equations 1) is low.

Furthermore, it is well-known that the photon energy required to enhance the formation of electron-hole pairs on a semiconductor is a function of its bandgap energy. As shown in section 3.2.3, the presence of Cu supports the utilization of the white light spectrum. On the other hand, intermediates (e.g., carbonate, CO₃²⁻) may be formed when the oxygen concentration increases.



Carbon dioxide is formed when the carbonate ion, CO₃²⁻, reacts with a hole (O^{*-}) and then with an electron.



3.4 Mathematical Correlation

CO degradation at each average seasonal temperature results from several parameters, namely: catalyst concentration (C_{Cu-TiO_2}), percent Cu loading (%Cu), light intensity (hv), gas flow rate (QG), and relative humidity (%RH). The regression analysis method using STAISTICA version 6.2 software were utilized to fit the experimental data for the photocatalytic reactor. The proposed model gives the following equation with a correlation factor of (0.9745) and variance equal to (0.9642). Figure 13 plots the experimental results vs. observed values of the empirical correlation.

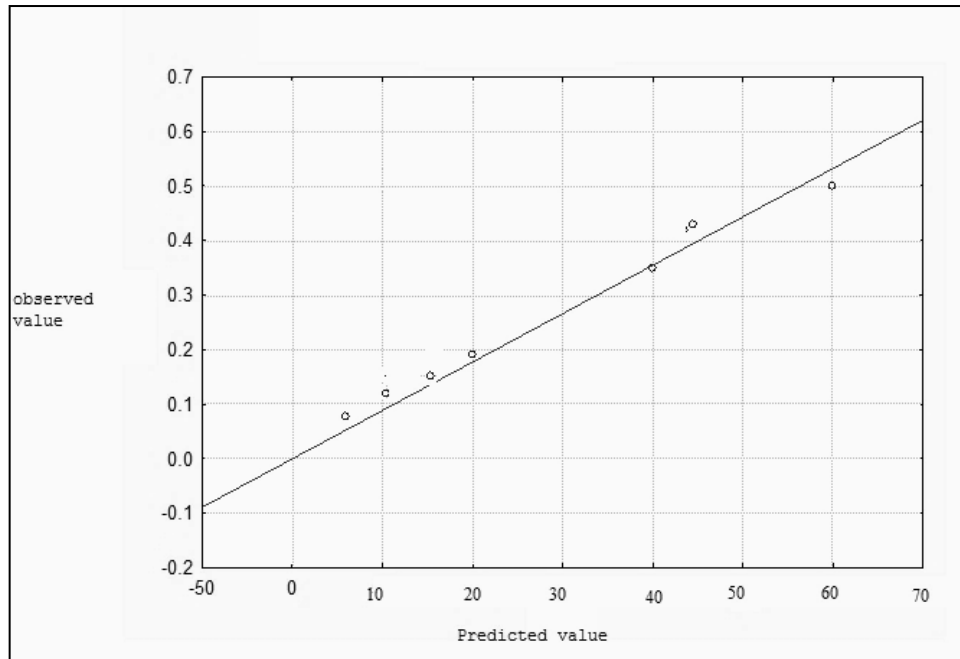


Figure 13: Observed values vs. predicted values for CO degradation (R %) in the photocatalytic reactor system

Then the regression Equation 12 in uncoded units becomes:

$$COX = 63.38 - 0.396 TiO_2 + 43.22 \%Cu - 2.665 HV - 5.98 QG - 0.4300 \%RH + 0.00742 TiO_2 * TiO_2 - 5.521 \%Cu * \%Cu + 0.03341 HV * HV - 0.0222 TiO_2 * \%Cu + 0.0041 \%Cu * HV \quad (12)$$

4. Conclusion

The present work was devoted to investigating experimentally the oxidation of gaseous CO emitted from an internal combustion engine using asphaltic pavement coated with Cu/TiO₂ nanoparticles irradiated by white light at ambient conditions. Cu doped Nano TiO₂ was used as the photocatalyst with narrow bandgap energy of 2.27 eV, which falls into the visible spectrum of wavelengths. This improved the photocatalytic activity and increased the (*OH) hydroxyl radical formation with active sites. Pollutants (CO) are adsorbed onto the catalyst surface, oxidized, and turned into final products (CO₂). The photocatalytic removal of CO in the exhaust gases was investigated under different experimental conditions. The comprehensive analysis of the removal of CO emissions yielded sufficient success in this study. Experimental results show that CO conversion is dependent positively on Cu loading, light intensity, and relative humidity. However, the gas flow rate showed a different trend. The optimum operating parameters were copper loading (3.6 wt. %), gas flow rate (1 L/min), relative humidity (30%), and light intensity of (35 W/m²) to ensure a photocatalytic oxidation efficiency of 56.4% after 3 hours of the process. The probable kinetic pathway of photo-oxidation of CO by *OH radicals were introduced for both high and low concentrations of oxygen in the ambient.

Acknowledgment

The authors are grateful to the Chemical Engineering Department, University of Technology, for providing space and facilities to conduct this work. Thanks are also due to the Ministry of Environment, for their assistance.

Author contribution

All authors contributed equally to this work.

Funding

This research received no specific grant from any funding agency in the public, commercial, or not-for-profit sectors.

Data availability statement

The data that support the findings of this study are available on request from the corresponding author.

Conflicts of interest

Authors declare that their present work has no conflict of interest with other published works.

References

- [1] J. A. Poole, C. S. Barnes, J. G. Demain, J. A. Bernstein, M. A. Padukudru, W. J. Sheehan, A. E. Nel, Impact of weather and climate change with indoor and outdoor air quality in asthma: A Work Group Report of the AAAAI Environmental Exposure and Respiratory Health Committee, *J. Allergy Clin. Immunol.*, 143 (2019) 1702-1710. <https://doi.org/10.1016/j.jaci.2019.02.018>
- [2] A. Talaiekhosravi, S. Rezaei, K. H. Kim, R. Sanaye, A. M. Amani, Recent advances in photocatalytic removal of organic and inorganic pollutants in air, *J. Clean. Prod.*, 278 (2021) 123895. <https://doi.org/10.1016/j.jclepro.2020.123895>
- [3] M. Salman, X. Long, L. Dauda, C. N. Mensah, S. Muhammad, Different impacts of export and import on carbon emissions across 7 ASEAN countries: A panel quantile regression approach, *Sci. Total Environ.*, 686 (2019) 1019-1029. <https://doi.org/10.1016/j.scitotenv.2019.06.019>
- [4] C. Callaghan, I. Fishtik, R. Datta, M. Carpenter, M. Chmielewski, A. Lugo, (2003). An improved microkinetic model for the water gas shift reaction on copper, *Surf. Sci.*, 541 (2003) 21-30. [https://doi.org/10.1016/S0039-6028\(03\)00953-1](https://doi.org/10.1016/S0039-6028(03)00953-1)
- [5] M. M. Khan, S. A. Ansari, D. Pradhan, M. O. Ansari, D. H. Han, J. Lee, M. H. Cho, Band gap engineered TiO₂ nanoparticles for visible light induced photoelectrochemical and photocatalytic studies, *J. Mater. Chem. A*, 2 (2014) 637-644. <https://doi.org/10.1039/c3ta14052k>
- [6] Z. Bielan, A. Sulowska, S. Dudziak, K. Siuzdak, J. Ryl, A. Zielińska-Jurek, Defective TiO₂ core-shell magnetic photocatalyst modified with plasmonic nanoparticles for visible light-induced photocatalytic activity, *Catalysts*, 10 (2020) 672. <https://doi.org/10.3390/catal10060672>
- [7] M. I. Litter, Heterogeneous photocatalysis: transition metal ions in photocatalytic systems, *Appl. Catal. B. Environ.*, 23 (1999) 89-114. [https://doi.org/10.1016/S0926-3373\(99\)00069-7](https://doi.org/10.1016/S0926-3373(99)00069-7)
- [8] X. Zhu, Q. Zhou, Y. Xia, J. Wang, H. Chen, Q. Xu, S. Chen, Preparation and characterization of Cu-doped TiO₂ nanomaterials with anatase/rutile/brookite triphasic structure and their photocatalytic activity, *J. Mater. Sci. Mater. Electron.*, 32 (2021) 21511-21524. <https://doi.org/10.1007/s10854-021-06660-5>
- [9] Z. Y. Shaniyan, M. F. Abid, K. A. Sukkar, Photodegradation of mefenamic acid from wastewater in a continuous flow solar falling film reactor, *Desalin. Water Treat.*, 210 (2021) 22-30. <https://doi.org/10.5004/dwt.2021.26581>
- [10] V. Krishnakumar, S. Boobas, J. Jayaprakash, M. Rajaboopathi, B. Han, M. Louhi-Kultanen, Effect of Cu doping on TiO₂ nanoparticles and its photocatalytic activity under visible light, *J. Mater. Sci. Mater. Electron.*, 27 (2016) 7438-7447. <https://doi.org/10.1007/s10854-016-4720-1>
- [11] A. S. Belousov, E. V. Suleimanov, Application of metal-organic frameworks as an alternative for metal oxide-based photocatalysts for production of industrially important organic chemicals, *Green Chem.*, 23 (2021) 6172-6204. <https://doi.org/10.1039/D1GC01690C>
- [12] S. B. Patil, P. S. Basavarajappa, N. Ganganagappa, M. S. Jyothi, A. V. Raghu, K. R. Reddy, Recent advances in non-metals-doped TiO₂ nanostructured photocatalysts for visible-light driven hydrogen production, CO₂ reduction and air purification, *Int. J. Hydrog. Energy*, 44 (2019) 13022-13039. <https://doi.org/10.1016/j.ijhydene.2019.03.164>
- [13] Q. Li, K. Wang, S. Zhang, M. Zhang, J. Yang, Z. Jin, Effect of photocatalytic activity of CO oxidation on Pt/TiO₂ by strong interaction between Pt and TiO₂ under oxidizing atmosphere, *J. Mol. Catal. A. Chem.*, 258 (2006) 83-88. <https://doi.org/10.1016/j.molcata.2006.05.030>
- [14] D. S. Selishchev, N. S. Kolobov, A. V. Bukhtiyarov, E. Y. Gerasimov, A. I. Gubanov, D. V. Kozlov, Deposition of Pd nanoparticles on TiO₂ using a Pd(acac)₂ precursor for photocatalytic oxidation of CO under UV-LED irradiation, *Appl. Catal. B: Environ.*, 235 (2018) 214-224. <https://doi.org/10.1016/j.apcatb.2018.04.074>
- [15] H. B. Tosun, A. Alver, E. Baştürk, Removal of Exhaust Gas with Advanced Solar Photocatalytic Asphalt Applications, *KSCE J. Civ. Eng.*, 26 (2022) 13-24. <https://doi.org/10.1007/s12205-021-0654-0>
- [16] X. Wu, J. Lang, Z. Sun, F. Jin, Y. H. Hu, Photocatalytic conversion of carbon monoxide: from pollutant removal to fuel production, *Appl. Catal. B: Environ.*, 295 (2021) 120312. <https://doi.org/10.1016/j.apcatb.2021.120312>

- [17] M. Al-Jemeli, M. A. Mahmoud, H. S. Majdi, M. F. Abid, H. M. Abdullah, A. A. AbdulRazak, Degradation of Anti-Inflammatory Drugs in Synthetic Wastewater by Solar Photocatalysis, Catalysts, 11 (2021) 1330. <https://doi.org/10.3390/catal11111330>
- [18] R. M. Mohamed, E. S. Aazam, Preparation and characterization of platinum doped porous titania nanoparticles for photocatalytic oxidation of carbon monoxide, J. Alloys Compd., 509 (2011) 10132-10138. <https://doi.org/10.1016/j.jallcom.2011.08.059>
- [19] J. Liu, R. Si, H. Zheng, Q. Geng, W. Dai, X. Chen, X. Fu, The promoted oxidation of CO induced by the visible-light response of Au nanoparticles over Au/TiO₂, Catal. Commun., 26 (2012) 136-139. <https://doi.org/10.1016/j.catcom.2012.05.011>
- [20] Y. Jiao, H. Jiang, F. Chen, RuO₂/TiO₂/Pt ternary photocatalysts with epitaxial heterojunction and their application in CO oxidation, ACS Catal., 4 (2014) 2249-2257. <https://doi.org/10.1021/cs5001174>
- [21] Y. Zhang, Q. Li, C. Liu, X. Shan, X. Chen, W. Dai, X. Fu, The promoted effect of a metal-organic frameworks (ZIF-8) on Au/TiO₂ for CO oxidation at room temperature both in dark and under visible light irradiation, Appl. Catal. B: Environ., <https://doi.org/10.1016/j.apcatb.2017.10.027>
- [22] K. Yang, K. Huang, L. Lin, X. Chen, W. Dai, X. Fu, Superior preferential oxidation of carbon monoxide in hydrogen-rich stream under visible light irradiation over gold loaded hedgehog-shaped titanium dioxide nanospheres: Identification of copper oxide decoration as an efficient promoter, J. Power Sources, 284 (2015) 194-205. <https://doi.org/10.1016/j.jpowsour.2015.03.003>
- [23] K. Yang, J. Liu, R. Si, X. Chen, W. Dai, X. Fu, Comparative study of Au/TiO₂ and Au/Al₂O₃ for oxidizing CO in the presence of H₂ under visible light irradiation, J. Catal., 317 (2014) 229-239. <https://doi.org/10.1016/j.jcat.2014.06.005>
- [24] H. Zheng, H. Yang, R. Si, W. Dai, X. Chen, X. Wang, X. Fu, The promoted effect of UV irradiation on the oxidation of CO in the presence and absence of hydrogen over the TiO₂-supported Pt/Co-B bicomponent catalyst, Appl. Catal. B: Environ., 105 (2011) 243-247. <https://doi.org/10.1016/j.apcatb.2011.04.027>
- [25] W. Dai, X. Zheng, H. Yang, X. Chen, X. Wang, P. Liu, X. Fu, The promoted effect of UV irradiation on preferential oxidation of CO in an H₂-rich stream over Au/TiO₂, J. Power Sources, 188 (2009) 507-514. <https://doi.org/10.1016/j.jpowsour.2008.12.028>
- [26] X. Tan, G. Cheng, X. Song, X. Chen, W. Dai, X. Fu, The promoting effect of visible light on the CO+ NO reaction over the Pd/N-TiO₂ catalyst, Catal. Sci. Technol., 9 (2019) 3637-3646. <https://doi.org/10.1039/C9CY00466A>
- [27] K. Huang, L. Lin, K. Yang, W. Dai, X. Chen, X. Fu, Promotion effect of ultraviolet light on NO+ CO reaction over Pt/TiO₂ and Pt/CeO₂-TiO₂ catalysts, Appl. Catal. B: Environ., 179 (2015) 395-406. <https://doi.org/10.1016/j.apcatb.2015.05.044>
- [28] Z. Jiang, Y. Ma, Y. Li, H. Liu, Highly effective UV-Vis-IR and IR photothermocatalytic CO abatement on Zn doped OMS-2 nanorods, Appl. Surf. Sci., 483 (2019) 827-834. <https://doi.org/10.1016/j.apsusc.2019.04.022>
- [29] Z. Lou, D. Yuan, F. Zhang, Y. Wang, Y. Li, L. Zhu, Fe₃Si assisted Co₃O₄ nanorods: A case study of photothermal catalytic CO oxidation under ambient solar irradiation, Nano Energy, 62 (2019) 653-659. <https://doi.org/10.1016/j.nanoen.2019.05.080>
- [30] A. A. AbdulRazak, Z. M. Shakor, S. Rohani, Optimizing Biebrich Scarlet removal from water by magnetic zeolite 13X using response surface method, J. Environ. Chem. Eng., 6 (2018) 6175-6183. <https://doi.org/10.1016/j.jece.2018.09.043>
- [31] Z. Majid, A. A. AbdulRazak, W. A. H. Noori, Modification of zeolite by magnetic nanoparticles for organic dye removal, Arab. J. Sci. Eng., 44 (2019) 5457-5474. <https://doi.org/10.1007/s13369-019-03788-9>
- [32] A. M. Alotaibi, B. A. Williamson, S. Sathasivam, A. Kafizas, M. Alqahtani, C. Sotelo-Vazquez, I. P. Parkin, Enhanced photocatalytic and antibacterial ability of Cu-doped anatase TiO₂ thin films: theory and experiment, ACS Appl. Mater. Interfaces, 12 (2020) 15348-15361. <https://doi.org/10.1021/acsami.9b22056>
- [33] M. F. Abid, S. T. Hamiedi, S. I. Ibrahim, S. K. Al-Nasri, Removal of toxic organic compounds from synthetic wastewater by a solar photocatalysis system, Desalin. Water Treat., 105 (2018) 119-125. <https://doi.org/10.5004/dwt.2018.22017>
- [34] M. Fadhil, Hydrodynamic Characteristics Effect of Foam Control in a Three-Phase Fluidized Bed Column, J. Pet. Sci. Eng., 3 (2012) E 158 - E 185. <https://doi.org/10.52716/jprs.v3i2.84>
- [35] JIS TR Z 0018, Photocatalytic Materials—Air Purification Test Procedure; Japanese Standards Association: Tokyo, Japan, 2002.

- [36] Hassan, M., Mohammad, L. N., Dylla, H., Cooper III, S. B., Mokhtar, A., & Asadi, S. A breakthrough concept in the preparation of highly-sustainable photocatalytic warm asphalt mixtures, In NSF Engineering Research and Innovation Conference, Atlanta, Georgia, 2011
- [37] M. F. Abid, M. Ebrahim, O. Nafi, L. Hussain, N. Maneual, A. Sameer, Designing and operating a pilot plant for purification of industrial wastewater from toxic organic compounds by utilizing solar energy, Korean J. Chem. Eng., 31 (2014) 1194-1203. <https://doi.org/10.1007/s11814-014-0052-0>
- [38] G. Hüsken, M. Hunger, H. J. H. Brouwers, Experimental study of photocatalytic concrete products for air purification, Build. Environ., 44 (2009) 2463-2474. <https://doi.org/10.1016/j.buildenv.2009.04.010>
- [39] M. Hassan, L. N. Mohammad, S. Asadi, H. Dylla, S. Cooper III, Sustainable photocatalytic asphalt pavements for mitigation of nitrogen oxide and sulfur dioxide vehicle emissions, J. Mater. Civ. Eng., 25 (2013) 365-371. [http://dx.doi.org/10.1061/\(ASCE\)MT.1943-5533.0000613](http://dx.doi.org/10.1061/(ASCE)MT.1943-5533.0000613)
- [40] Ohama, Y., & Van Gemert, D. Application of titanium dioxide photocatalysis to construction materials: state-of-the-art report of the RILEM Technical Committee 194-TDP, Springer Science & Business Media, 2011. <https://doi.org/10.1007/978-94-007-1297-3>
- [41] W. A. Jacoby, D. M. Blake, R. D. Noble, C. A. Koval, Kinetics of the oxidation of trichloroethylene in air via heterogeneous photocatalysis, J. Catal., 157 (1995) 87-96. <https://doi.org/10.1006/jcat.1995.1270>
- [42] T. H. Lim, S. M. Jeong, S. D. Kim, J. Gyenis, Photocatalytic decomposition of NO by TiO₂ particles, J. Photochem. Photobiol. A: Chem., 134 (2000) 209-217. [https://doi.org/10.1016/S1010-6030\(00\)00265-3](https://doi.org/10.1016/S1010-6030(00)00265-3)
- [43] J. V. S. de Melo, G. Trichês, P. J. P. Gleize, J. Villena, Development and evaluation of the efficiency of photocatalytic pavement blocks in the laboratory and after one year in the field, Constr. Build. Mater., 37 (2012) 310-319. <https://doi.org/10.1016/j.conbuildmat.2012.07.073>
- [44] D. V. Raorane, P. S. Chavan, S. R. Pednekar, R. S. Chaughule, Green and rapid synthesis of copper-doped TiO₂ nanoparticles with increased photocatalytic activity, Sci. Eng. Pub. Comp. Adv. Chem. Sci., 6 (2017) 13-20. <https://doi.org/10.14355/sepacs.2017.06.002>
- [45] L. S. Yoong, F. K. Chong, B. K. Dutta, Development of copper-doped TiO₂ photocatalyst for hydrogen production under visible light, Energy, 34 (2009) 1652-1661. <https://doi.org/10.1016/j.energy.2009.07.024>
- [46] N. Z. Searle, R. C. Hirt, Ultraviolet spectral energy distribution of sunlight, J. Opt. Soc. Am., 55 (1965) 1413-1421. <https://doi.org/10.1364/JOSA.55.001413>